JOURNAL OF SOLID STATE CHEMISTRY 93, 17–29 (1991)

White Light Emitting Glasses

ZHANG JIN CHAO, C. PARENT, G. LE FLEM, AND P. HAGENMULLER

Laboratoire de Chimie du Solide du CNRS, Université de Bordeaux I, 351 cours de la Libération, 33405 Talence Cedex, France

Received April 13, 1990; in revised form January 30, 1991

For the first time vitreous materials capable of generating "white light" by simultaneous emission of blue, green, and red emitting fluorescent centers have been produced. These glasses are B_2O_3-based and contain Ce^{3+}, Tb^{3+}, and Mn^{2+} as activators. Both chromaticity coordinates and luminescence intensity vary vs glass composition and activator concentration. The spectroscopic properties of singly, doubly, and triply doped glasses are reported. Ce^{3+} shows a broad-band emission centered at the border between UV and visible light domains. Moreover, this ion acts as a donor in codoped glasses, transferring part of its energy to Tb^{3+} and Mn^{2+}, whose luminescence occurs respectively in the green and red parts of the visible. The mechanisms of the various energy transfers observed have been investigated by a detailed kinetic investigation. © 1991 Academic Press, Inc.

Introduction

Most fluorescence lamps use a calcium halophosphate apatite phosphor with the generic formula $Ca_5(PO_4)_3(F,Cl):Sb^{3+},Mn^2$ (*1*). With this material white light is generated using a single phosphor. In low pressure mercury vapor lamps the 254-nm emission excites Sb^{3+}, which gives a broad band emission in the blue region of the visible spectrum and transfers a part of its excitation energy to Mn^{2+}, whose broad-band emission is located in the yellow orange. A lamp efficiency of 80 lm/W is obtained.

In 1971, Koedan and Opstelten (*2*) and Thornton (*3*) showed that a high efficiency could be obtained by mixing three phosphors emitting in narrow wavelength ranges centered at 450, 550, and 610 nm, respectively. Such a blend was practically realized for the first time by Verstegen *et al.* by combining the blue emission of $BaMg_2Al_{16}O_{27}:Eu^{2+}$, the green emission of $CeMgAl_{11}O_{19}:Tb^{3+}$, and the red one of $Y_2O_3:Eu^{3+}$ (*4*).

In a more recent development, the borates $LnMgB_5O_{10}$ (Ln = rare earth) doped with cerium and terbium (*5*), cerium and manganese (*6*), or cerium, terbium, and manganese (*7*) have been shown to give efficient green, red, and white emitting phosphors. Moreover, in these borates Gd^{3+} can play an important role as a sensitizer (*8–10*).

In this context, we report the first investigation of luminescent glasses able to generate white light under UV excitation.

The selected glasses contain about 63 mole% B_2O_3. They are easy to produce and their thermal and structural properties have been thoroughly investigated.

The activators introduced in the glasses were the Ce^{3+}, Tb^{3+}, and Mn^{2+} ions. They fulfill the following requirements:

(i) Chemical compatibility is observed in borate matrices.

0022-4596/91 $3.00
Copyright © 1991 by Academic Press, Inc.
All rights of reproduction in any form reserved.

(ii) Subjected to appropriate crystal fields, they can emit respectively in the blue, the green, and the red parts of the spectrum.

(iii) Their luminescence quantum yield can be high.

Ce^{3+} efficiently sensitizes Tb^{3+} and Mn^{2+} under UV excitation.

We shall describe successively: (I) the experimental procedure; (II) the luminescence of cerium-doped glasses; (III) the luminescence of terbium-doped glasses; (IV) the luminescence of manganese-doped glasses; (V) the sensitization of Tb^{3+} luminescence by Ce^{3+} ions in cerium-terbium codoped glasses; (VI) the sensitization of Mn^{2+} luminescence by Ce^{3+} ions in cerium-manganese codoped glasses; and (VII) the luminescence of glasses activated by Ce^{3+}, Tb^{3+} and Mn^{2+}.

I. Experimental Procedure

Materials

The glasses investigated had the nominal base composition $67B_2O_3$, $15M_2O$ (M = Li, Na, or K), (10-z) RO (R = Mg, Ca, or Ba), (5-x-y) La_2O_3, $2Al_2O_3$, $1As_2O_3$, xCe_2O_3, yTb_2O_3, $zMnO$ with $x \leq 2$, $y \leq 4$, and $z \leq 10$. As_2O_3 was introduced to prevent Ce^{3+} and Tb^{3+} from possible oxidation.

The samples were prepared using alkali, alkali-earth, and manganous carbonates (Merck, 99.5%) and B_2O_3 (Merck, 99.5%), Al_2O_3 (Cerac, 99.99%), La_2O_3, CeO_2, and Tb_4O_7 (Rhone Poulenc, 99.99%) oxides. The dry starting materials were carefully mixed in the selected proportions, introduced into a vitreous carbon crucible, and decarbonated between 500 and 650°C. Then the temperature was raised to 1200–1350°C and held at that value for 1 hr under controlled nitrogen flow. The molten glasses were poured into a preheated graphite mold, annealed at 510°C for 5 hr, and cooled down to room temperature at 0.5°C/min.

The basic characteristics of these glasses have been previously reported (*11*).

Spectroscopic Measurements

The absorption spectra were recorded at room temperature using a Cary 17 spectrophotometer. The spectral resolution was about 0.2 nm.

The emission spectral distribution was analyzed with a Jobin–Yvon HRS3 monochromator and detected using a R928 Hamamatsu photomultiplier. The excitation source was a high-pressure xenon lamp emitting between 200 and 1000 nm.

The fluorescence decays have been recorded under the pulsed excitation of a 803 A Sopra nitrogen laser emitting 8-ns pulses at 337 nm. The signals were detected with a RTC 56 DUVP photomultiplier mounted on a Jobin–Yvon HRS 640 monochromator and connected to a PAR M 162/165 boxar averager.

Except in some particular cases, the composition of the samples will be labeled by indicating only the nature of alkali and alkali-earth elements and the proportion of activators used, e.g., (Li, Ba, 1% Ce_2O_3, 1% Tb_2O_3) corresponds to $67B_2O_3$, $15Li_2O$, $10BaO$, $3La_2O_3$, $2Al_2O_3$, $1As_2O_3$, $1Ce_2O_3$, $1Tb_2O_3$.

II. The Luminescence of Cerium-Doped Glasses

Absorption

Figure 1 compares the absorption spectra of samples without activator and those containing different cerium concentrations. Because the $4f \rightarrow 5d$ transition in Ce^{3+} is allowed, there is high absorptivity in the near UV.

Emission

When the glasses are activated by cerium alone, they exhibit a broad-band emission corresponding to the transitions between

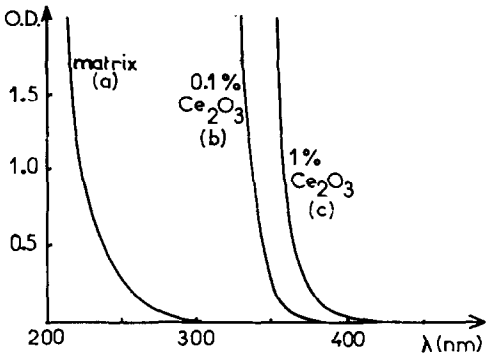

FIG. 1. Absorption spectra of various (Li, Ba, $x\%$ Ce_2O_3) glasses, at T = 300 K (thickness, 0.3 cm).

the lowest crystal field components of the $5d$ band and the $^2F_{7/2}$ and $^2F_{5/2}$ $4f$ levels. For (Li, Ba, 1% Ce_2O_3) the emission maximum is located around 380 nm.

Modification of the excitation wavelength has no influence on the spectral distribution of cerium fluorescence. On the contrary, a red shift of the emission maximum is observed:

(i) by replacing given alkali or alkali-earth elements by more electropositive ones, e.g., Li by Na (Fig. 2A);

(ii) by increasing the modifier ion concentration (Fig. 2B).

This evolution is consistent obviously with a change of the crystal field at the cerium multisites (*12, 13*), but also with a lowering of the emitting $5d$ levels (nephelauxetic effect). Ce–O bonds are in competition either with more ionic metal–oxygen bonds (case (i)) or eventually with more ionic boron–oxygen bonds (case (ii)) resulting from the formation of (BO_4) tetrahedral units at the expense of (BO_3) triangles.

Excitation

The excitation spectrum of Ce^{3+} recorded for the (Li, Ba, 1% Ce_2O_3) glass is shown in Fig. 3. This spectrum consists of a broad band peaking at about 330 nm. Its overlapping with the emission spectrum results in an important reabsorption of emitted photons of higher energy. For samples with enough cerium this effect leads to a red shift of the light emitted by a block, in comparison with that observed for powdered glass of identical composition.

Lifetime of 5d-Excited States

The $\tau_{Ce^{3+}}$ lifetimes of the $5d$-excited states have been deduced from the decay curves of the $5d \rightarrow {}^2F_{7/2}, {}^2F_{5/2}$ emission. The curves are approximately a single exponential and

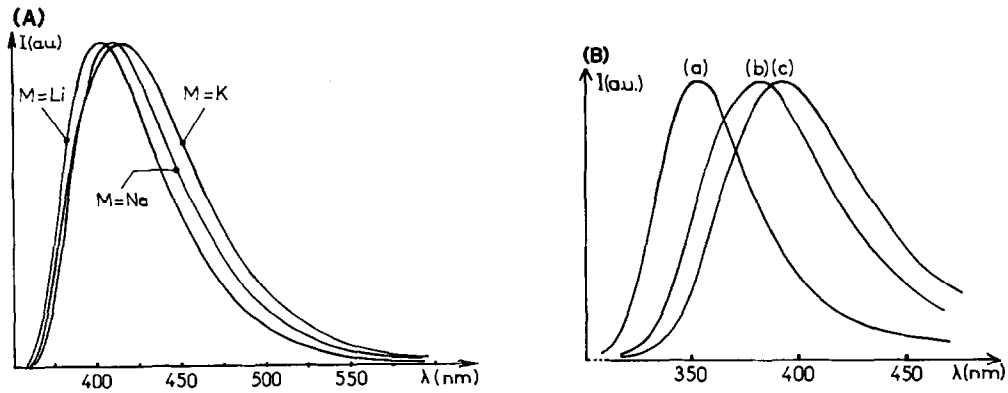

FIG. 2. Shift of the Ce^{3+} emission band under a 254-nm excitation (ground glasses, T = 300 K), (A) for the (M, Ba, 1% Ce_2O_3) glasses, as a function of the nature of the M alkali element; (B) as a function of the modifier ion concentration: (a) $80B_2O_3$, $10.5Li_2O$, $6BaO$, $1Al_2O_3$, $0.5As_2O_3$, $2La_2O_3$, $1Ce_2O_3$; (b) (Li, Ba, 1% Ce_2O_3); (c) $60B_2O_3$, $21.5Li_2O$, $11BaO$, $2Al_2O_3$, $0.5As_2O_3$, $4La_2O_3$, $1Ce_2O_3$.

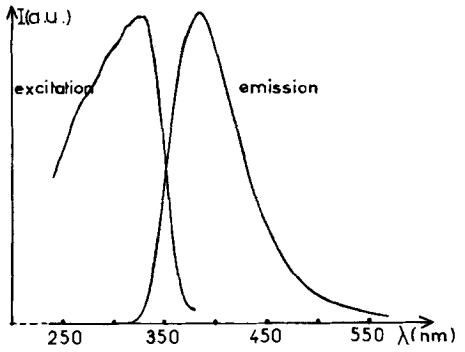

FIG. 3. Overlapping between Ce^{3+} excitation (λ_{em} = 400 nm) and emission (λ_{exc} = 254 nm) spectra for a (Li, Ba, 1% Ce_2O_3) ground glass, at T = 300 K.

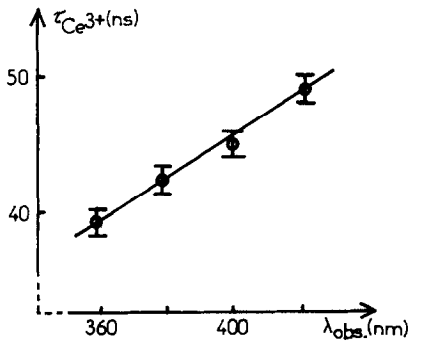

FIG. 4. Variation of the $\tau_{Ce^{3+}}$ lifetime in a (Li, Ba, 1% Ce_2O_3) vitreous block as a function of the emission wavelength, λ_{obs}, selected for luminescence decay recording, under a pulsed 337-nm excitation (T = 300 K).

the time dependence of the $I(t)$ emission intensity can be written as

$$I(t) = I_0 \exp(-t/\tau_{Ce^{3+}}),$$

where I_0 is the emission intensity at $t = 0$.

For such samples with a low activator content, the lifetimes are found to be roughly independent of Ce^{3+} concentration, which excludes Ce–Ce transfer. In contrast, the decay is longer when the observation wavelength of the luminescence increases (Fig. 4). This evolution can be related to the reabsorption phenomenon: during the decay the low energy emission is continuously fed by the energy provided by the radiative transfer.

III. The Luminescence of Terbium-Doped Glasses

Figure 5 shows the absorption spectrum of the (Li, Ba, 0.1% Tb_2O_3) glass. The long-wavelength absorption region exhibits the characteristic Tb^{3+} lines resulting from the forbidden $4f$–$4f$ transitions. At higher energy the intense band corresponds to the permitted $4f \rightarrow 5d$ transitions. The intensity is about 3000 times as high as that of the forbidden lines.

The emission spectrum of the same sample under 254-nm excitation consists mainly of the Tb^{3+} emission from the $^5D_4$ level with the usual $^5D_4 \rightarrow {}^7F_5$ intense green luminescence (Fig. 6).

Under pulsed 337-nm excitation the decay of the $^5D_4 \rightarrow {}^7F_5$ emission appears to be exponential and the $^5D_4$ lifetime is about 2.5 ms, regardless of the activator concentration, which illustrates the absence of self concentration quenching.

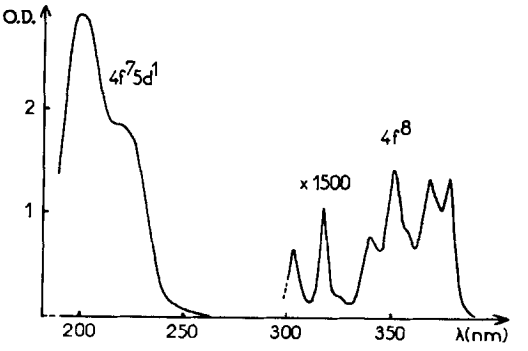

FIG. 5. Tb^{3+} absorption spectrum for a (Li, Ba, 1% Tb_2O_3) flat glass of 0.075 cm thickness.

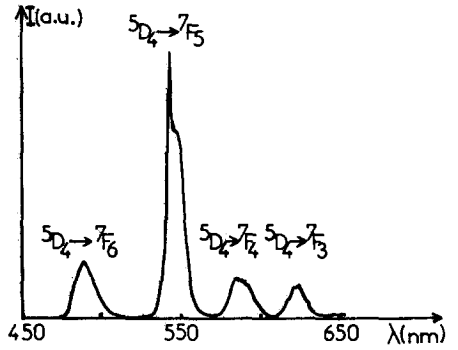

FIG. 6. Tb^{3+} emission spectrum for a (Li, Ba, 1% Tb_2O_3) glass under 254-nm excitation at T = 300 K.

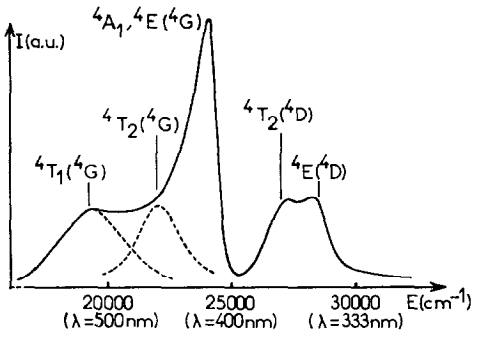

FIG. 8. Mn^{2+} excitation spectrum of a (Li, Ba, 2% MnO) vitreous block, for the 650-nm $^4T_1(^4G) \rightarrow {}^6A_1$ emission, at T = 4.2 K.

IV. The Luminescence of Manganese-Doped Glasses

Absorption

The absorption spectrum of the (Li, Ba, 10% MnO) glass is shown in Fig. 7. It is very similar to that previously published by K. Bingham and S. Parke for the glass of $1Na_2O$, $4B_2O_3$ composition (*14*) and explains the beige–pink color of the samples, which is more or less pronounced according to the activator concentration.

In such a spectrum, the large inhomogeneous broadening of the bands, due to the presence of multisite activators, does not allow quantitative calculations. In contrast the crystal field and the Racah parameters of Mn^{3+} may be deduced from the excitation spectrum for which these bands are relatively well-resolved. As an example the excitation spectrum at 4.2 K of a (Li, Ba, 2% MnO) glass for the 650-nm luminescence is given in Fig. 8.

For the borates the validity of the ligand field theory is quite unequivocal. The excitation bands have been identified from the Tanabe–Sugano energy level diagram for a d^5 configuration (*15*) (Fig. 9). The crystal field

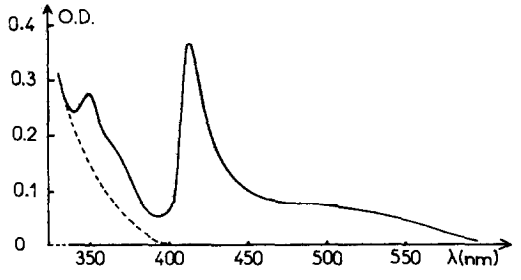

FIG. 7. Room temperature absorption spectrum of a (Li, Ba, 10% MnO) flat glass (thickness: 0.38 cm). The dotted line represents the matrix absorption.

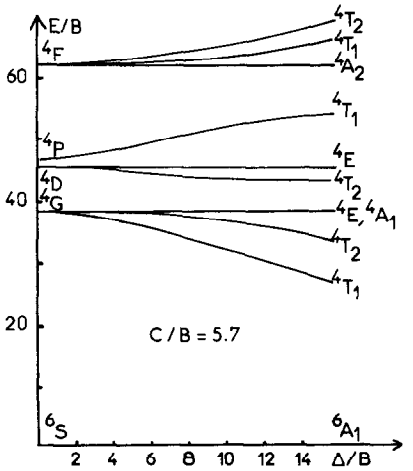

FIG. 9. Evolution of Mn^{2+} energy levels as a function of the crystal field strength, for C/B supposed to be 5.7.

TABLE I

Mn^{2+} Excitation Bands of a (Li, Ba, 2% MnO) Glass for a $^4T_1(^4G) \rightarrow {}^6A_1$ Emission at T = 4.2 K: Calculated and Observed Positions

Excitation band $^6A_1 \rightarrow$	Calculated position (cm^{-1})	Experimental position (cm^{-1})
$^4T_1(^4G)$	19,481	19,490 ± 50
$^4T_2(^4G)$	22,837	22,500 ± 500
$^4E, {}^4A_1(^4G)$	24,094	24,095 ± 10
$^4T_2(^4D)$	27,160	27,170 ± 50
$^4E(^4D)$	28,474	28,475 ± 50

strength Δ and the Racah parameters B and C have been calculated with the weak field matrices of the quartet levels given by K. Bingham and S. Parke (*14*). A least square fitting leads to

$$\Delta = 7100\ cm^{-1},\ B = 625\ cm^{-1},$$
$$\text{and } C = 3570\ cm^{-1}.$$

The calculated and observed positions of the excitation bands are listed in Table I.

The values obtained agree with those previously published for the ($1Na_2O$, $4B_2O_3$) glass by Bingham *et al.* (Δ = 6800 cm^{-1}, B = 630 cm^{-1}, C = 3610 cm^{-1}) and also with the data of a recent and detailed investigation of P. E. Menassa *et al.* who found for a boron-rich glass (*16*),

$$\Delta = 6500\ cm^{-1},\ B = 633\ cm^{-1},$$
$$\text{and } C = 3610\ cm^{-1}.$$

All results are consistent with the location of Mn^{2+} in octahedral sites (*16, 17*).

Emission

The emission spectra of (Li, Ba, z% MnO) glasses for various manganese concentrations are shown in Fig. 10. The visual emission varies from orange to red as the activator rate increases. The emission intensity reaches a maximum for z = 2 and decreases thereafter. The most probable reason for this is an efficient energy transfer between two activators. In this scheme, the lower energy emission would be enhanced at the expense of the higher energy one.

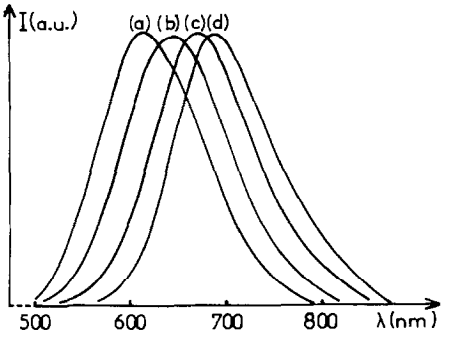

FIG. 10. Mn^{2+} emission normalized spectra of (Li, Ba, z% MnO) glasses for various manganese concentrations, under 410-nm excitation, at T = 300 K. (a) z = 0.2, (b) z = 2, (c) z = 5, (d) z = 10.

The orange–red luminescence confirms also the location of Mn^{2+} in octahedral sites.

Luminescence Decay

Figure 11 shows the Mn^{2+} emission decay for the (Li, Ba, z% MnO) glasses for two

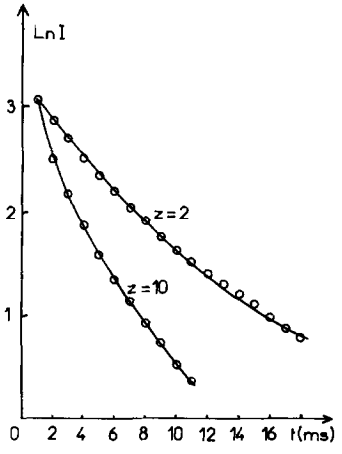

FIG. 11. Mn^{2+} $^4T_1(^4G) \rightarrow {}^6A_1$ emission decay (λ_{em} = 650 nm) at room temperature under a pulsed 337-nm excitation, for (Li, Ba, z% MnO) vitreous blocks (z = 2 and z = 10).

activator concentrations: $z = 2$ and $z = 10$. Under 337-nm pulsed excitation a nonexponential behavior is always observed due to the existence of more than one site. Therefore, the lifetime values are given for the time of the first e-folding intensity ($z = 2$, $\tau = 5.7$ ms, $z = 5$, $\tau = 3.9$ ms, $z = 10$, $\tau = 2.5$ ms).

The lifetime is emission wavelength independent and begins to decrease for samples with $z > 2$. This latter evolution can also be related to the self concentration quenching.

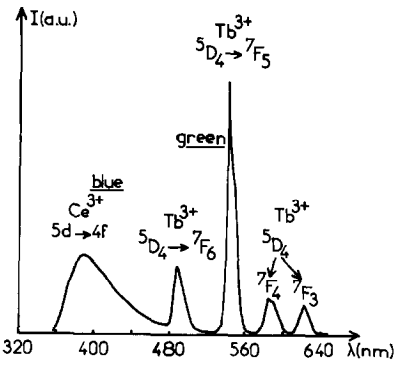

FIG. 13. Spectral distribution of the emission of a (Li, Ba, 1% Ce_2O_3, 0.5% Tb_2O_3) vitreous block under 254-nm excitation at room temperature.

V. Sensitization of Tb^{3+} Luminescence by Ce^{3+} Ions in Cerium–Terbium-Codoped Glasses

Simultaneous Blue and Green Emissions under 254-nm Excitation

Ce^{3+} in phosphors efficiently sensitizes terbium emission under excitation by the UV light emitted by the excited Hg atoms in fluorescent lamps. To have a high yield, codoped materials need an efficient $Ce^{3+} \rightarrow Tb^{3+}$ transfer (*18*).

The main requirement for such a transfer is a good overlap between terbium excitation and cerium emission spectra (*19, 20*). The positions of the Tb^{3+} $4f^8$ levels are relatively insensitive to the matrix. In contrast, as previously shown in Section II, the cerium emission spectrum depends on the glass composition and can be modified by the composition of the host material. This composition must be selected so as to induce partial overlapping of sensitizer emission and acceptor excitation spectra in order to allow both cerium emission and efficient $Ce^{3+} \rightarrow Tb^{3+}$ transfer. An example is the glass of composition (Li, Ba, 1% Ce_2O_3, 1% Tb_2O_3) (Fig. 12).

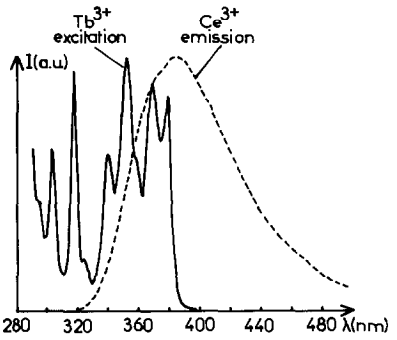

FIG. 12. Partial overlapping between Ce^{3+} emission and Tb^{3+} excitation spectra for a powdered (Li, Ba, 1% Ce_2O_3, 1% Tb_2O_3) glass, at $T = 300$ K (normalized spectra).

The spectral distribution of the emission of a vitreous block with similar composition under 254-nm excitation is shown in Fig. 13. Ce^{3+} and Tb^{3+} emissions are simultaneously observed.

Mechanism of the $Ce^{3+} \rightarrow Tb^{3+}$ Transfer

The mechanism of the sensitization of the Tb^{3+} luminescence by Ce^{3+} can be analyzed using the approach of Dexter's theory (*19*). Usually the interaction between Ce^{3+} and Tb^{3+} is of an electric dipole–dipole nature for low acceptor concentrations.

Figure 14 compares the Ce^{3+} decays for two vitreous blocks either doped only with Ce^{3+} ($x = 1$, $y = 0$) or codoped with Ce^{3+} and Tb^{3+} ($x = 1$, $y = 3$). At $y = 0$ the slight deviation from a pure exponential curve results from the inhomogeneous site distribu-

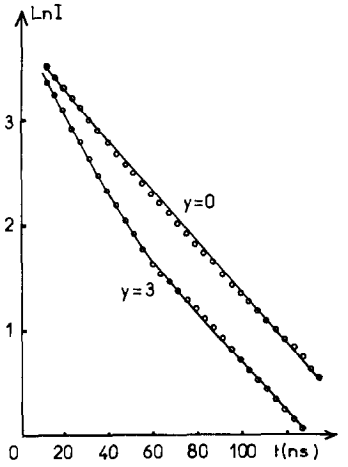

FIG. 14. Ce^{3+} luminescence decay under pulsed 337-nm excitation for two (Li, Ba, 1% Ce_2O_3, y% Tb_2O_3) vitreous blocks at T = 300 K.

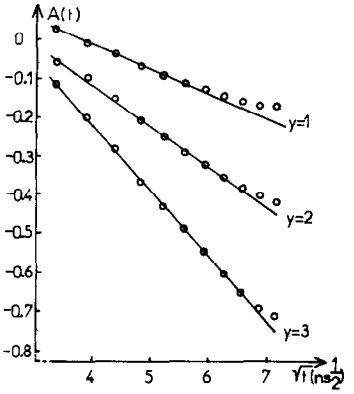

FIG. 15. Evolution of the first part of the Ce^{3+} emission decay curve as a function of terbium concentration, for codoped (Li, Ba, 1% Ce_2O_3) vitreous blocks (T = 300 K).

tion. Introduction of Tb^{3+} (x = 1, y = 3) accelerates the decay only during the first 50 ns.

Assuming a dipole–dipole radiationless energy transfer, the donor decay curve may be written as (*21–25*).

$$I(t) = I_0 \exp[-(t/\tau_0) - \pi(t)]. \quad (1)$$

τ_0 is the excited state lifetime of the donor in the absence of any interaction and the $\pi(t)$ function describes the influence of the interactions between activators during the decay. The time dependence of $\pi(t)$ turns out to be quite different depending on whether or not energy migration occurs over the donor subsystem (*21, 22*). In the quasi-statistical limit, i.e., with no energy migration over the donor Ce^{3+} ions, $\pi(t)$ has a Forster-like time dependence (*23*),

$$\pi(t) = \gamma\sqrt{t}, \quad (2)$$

with

$$\gamma = \tfrac{4}{3}\pi^{3/2} N_A \sqrt{C_{DA}}, \quad (3)$$

where N_A is the acceptor density of the sample and C_{DA} the donor–acceptor interaction parameter related to the P_{DA} interaction probability and to the R distance between donor and acceptor by the relation

$$P_{DA} = C_{DA}/R^6.$$

As the concentration of the Tb^{3+} acceptor increases, Eq. (1) may be written as

$$A(t) = |\mathrm{LnI}| - |\mathrm{LnI}|_{y=0} = -\gamma\sqrt{t} = c^{te}. \quad (4)$$

As shown in Fig. 15, the $A(t) = f(\sqrt{t})$ variation is linear up to 40 ns. According to Formula (3), γ varies linearly with the terbium concentration (Fig. 16) and a calculation of the intrinsic parameter characteriz-

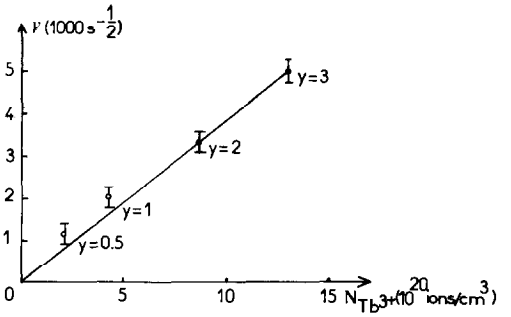

FIG. 16. γ_{Ce-Tb} variations vs Tb^{3+} concentration for the (Li, Ba, 1% Ce_2O_3, y% Tb_2O_3) glasses.

ing the $Ce^{3+} \rightarrow Tb^{3+}$ transfer leads to $C_{DA(Ce^{3+} \rightarrow Tb^{3+})} = 2.8 \times 10^{-37}$ cm^6 sec^{-1}.

These values are much higher than those previously found by C. Lurin *et al.* for the $Nd^{3+} \rightarrow Nd^{3+}$ and $Nd^{3+} \rightarrow Yb^{3+}$ transfers in the same vitreous matrices (*26*)

$$C_{DD}(Nd^{3+} \rightarrow Nd^{3+}) = 1.6 \times 10^{-39}\,\text{cm}^6\,\text{sec}^{-1}$$

$$C_{DA}(Nd^{3+} \rightarrow Yb^{3+}) = 6 \times 10^{-39}\,\text{cm}^6\,\text{sec}^{-1}$$

The allowed electric dipole character of the Ce^{3+} emission transitions explains the higher value of the $C_{DA(Ce^{3+} \rightarrow Tb^{3+})}$ parameter as compared to those resulting from donor and acceptor ions involving both only $4f$–$4f$ transitions.

The probability of the Ce–Tb transfer P_{DA} can be roughly estimated by assuming purely exponential decay curves within the first 40 ns, using the relation

$$P_{DA}(Ce^{3+} \rightarrow Tb^{3+}) = \frac{1}{\tau} - \frac{1}{\tau_0},$$

where τ_0 is the Ce^{3+} excited state lifetime for the single-doped (Li, Ba, 1% Ce_2O_3) glass and τ is the lifetime for the cerium and terbium-codoped glass. In this approximation $\tau_0 = 40$ ns, $\tau = 27$ ns and $P_{DA}(Ce^{3+} \rightarrow Tb^{3+}) = 1.2 \times 10^7$ sec^{-1}. By introducing this value in the $P_{DA} = C_{DA}/R^6$ relation, we obtain $R_m = 5.3$ Å, R_m being the mean Ce–Tb distance.

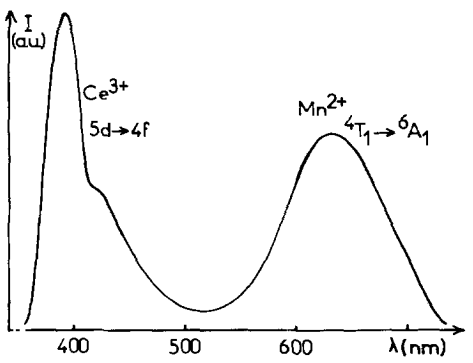

FIG. 17. Emission spectrum of a (Li, Ba, 1% Ce_2O_3, 2% MnO) vitreous block under 254-nm excitation at T = 300 K.

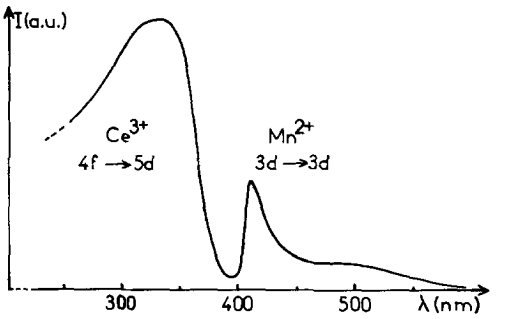

FIG. 18. Excitation spectrum of a (Li, Ba, 1% Ce_2O_3, 2% MnO) ground glass for the Mn^{2+} emission at 650 nm (T = 300 K).

VI. Sensitization of Mn^{2+} Luminescence by Ce^{3+} Ions in Cerium–Manganese-Codoped Glasses

The glasses which contain both Ce^{3+} and Mn^{2+} exhibit the blue Ce^{3+} and the red Mn^{2+} emission under 254-nm excitation (Fig. 17). The red emission is expected to result from a $Ce^{3+} \rightarrow Mn^{2+}$ transfer as in these borates Mn^{2+} ions cannot be directly excited at such a wavelength. The excitation spectrum for the manganese emission (λ_{em} = 650 nm) of codoped glasses consists of the Mn^{2+} narrow bands and of a broad band around 310 nm due to the $4f \rightarrow 5d$ transitions within the Ce^{3+} ion (Fig. 18). In addition, the Ce^{3+} emission and Mn^{2+} excitation spectra of singly doped Ce^{3+} or Mn^{2+} glasses exhibit good overlapping.

Mechanisms of the $Ce^{3+} \rightarrow Mn^{2+}$ Energy Transfer

In the codoped glasses the Ce^{3+} emission intensity is strongly reduced on the low energy side of the emission band between 400 and 450 nm, compared to that observed for the singly Ce^{3+}-doped glasses (Fig. 17 and Fig. 2). Thereby a radiative transfer is likely

to occur, a part of the photons emitted by Ce^{3+} are reabsorbed by Mn^{2+} via the $^6A_1 \rightarrow {}^4A_1, {}^4E$ transitions. However, the whole donor → acceptor transfer is not restricted to this radiative process. In presence of Mn^{2+}, the Ce^{3+} emission decay is strongly accelerated during the first 40 nsec (Fig. 19).

The corresponding $Ce^{3+} \rightarrow Mn^{2+}$ transfer can be analyzed in the context of Dexter's theory, using the formalism introduced in the previous section.

For the pure Ce^{3+} glass, the emission decay curve may be considered as exponential in a first approximation. It may be written as

$$I_1 = I_{01} \exp(-t/\tau_0),$$

where τ_0 is the lifetime of the cerium emitting levels. Introduction of Mn^{2+} leads to a modification of the decay curve during the initial period which may be represented as $I_2 = I_{02} \exp(-t/\tau_0 - \gamma\sqrt{t})$. A linear variation of the $[LnI_2-LnI_1]$ function vs t is effectively found (Fig. 20). In agreement with Eq. (3), γ varies linearly with the acceptor concentration and $C_{DA(Ce^{3+}\rightarrow Mn^{2+})} = 5.4 \times 10^{-37}$ cm^6 s^{-1}. Thus this $Ce^{3+} \rightarrow Mn^{2+}$ transfer is approximately twice as efficient as the $Ce^{3+} \rightarrow Tb^{3+}$ transfer found in the previous section.

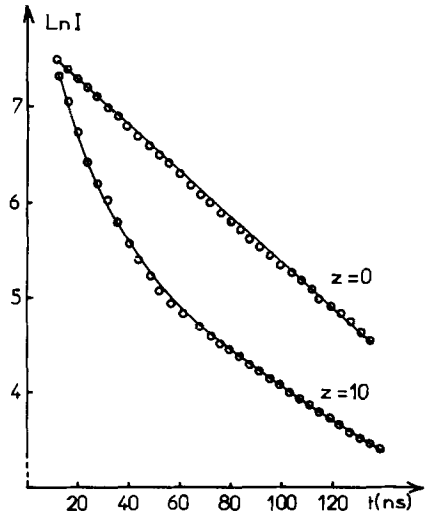

FIG. 19. Ce^{3+} emission decays for two (Li, Ba, 1% Ce_2O_3, z% MnO) vitreous blocks under pulsed 337-nm excitation at T = 300 K.

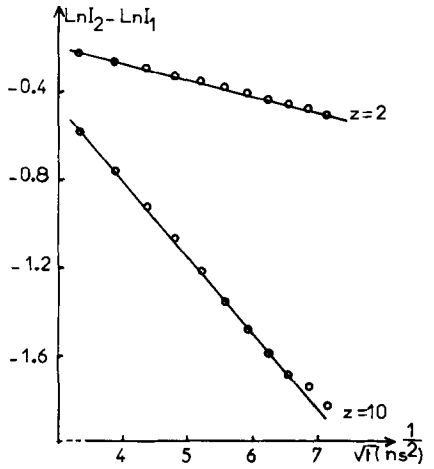

FIG. 20. Evolution of the first part of the Ce^{3+} emission decay curve as a function of manganese concentration for codoped (Li, Ba, 1% Ce_2O_3, z% MnO) vitreous blocks (T = 300 K).

Assuming, as in Section V, a roughly linear time variation in the initial part of the curve of Fig. 19 corresponding to $z = 10$, the τ lifetime of the Ce^{3+} excited states is about 17 ns. As a consequence the $Ce^{3+} \rightarrow Mn^{2+}$ transfer probability can be estimated at 3.4×10^7 s^{-1}, which leads to a Ce–Mn mean distance $R_m \simeq 5$ Å. This value is also realistic if one considers the ionic radii of Mn^{2+} (C.N. VI) and Ce^{3+} (C.N. VIII) which are respectively 0.67 Å and 1.14 Å.

Nevertheless, the involvement of an exchange mechanism between cerium and manganese cannot be excluded. Such an effect was previously observed between antimony and manganese in fluorophosphate phosphors (*27*). It could give a similar form for the early decay behavior. The determination of the true mechanism needs a com-

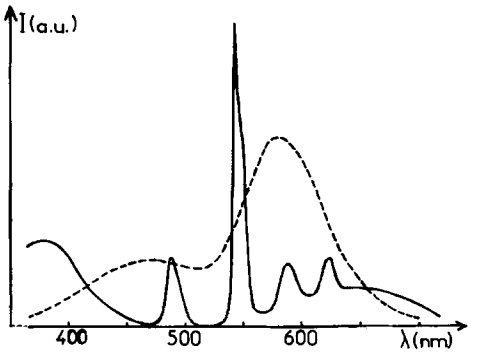

FIG. 21. Comparison between the spectral distributions of the emissions, under a similar 254-nm excitation, of the (Li, Ba, 1% Ce_2O_3, 1% Tb_2O_3, 1% MnO) ground glass (—) and of the standard calcium halophosphate phosphor $Ca_5(PO_4)_3$ (F, Cl): Sb^{3+}, Mn^{2+} (---).

plementary investigation involving quantum yield (*21*) and magnetic susceptibility measurements.

VII. The Luminescence of Glasses Simultaneously Activated by Ce^{3+}, Tb^{3+}, and Mn^{2+}

The borate glasses activated by Ce^{3+}, Tb^{3+}, and Mn^{2+} ions show simultaneously the blue cerium emission, the green terbium emission, and the red manganese emission. The combination of these emissions provides white light under 365-nm excitation (i.e., that of a high-pressure mercury vapor lamp) and a yellow-green light under 254-nm excitation (low-pressure mercury vapor lamp).

The evolution of the emission color has been systematically investigated as a function of the excitation wavelength for the (Li, Ba, 1% Ce_2O_3, 1% Tb_2O_3, 1% MnO) glass. The global emission was characterized by the variation of its chromaticity coordinates in the C.I.E. chromaticity diagram. The intensity of the cerium emission decreases as the excitation wavelength decreases. It results in a continuous shift of the color emission from the white to the yellow–green region. The decrease of the Ce^{3+} quantum yield under high excitation energy is generally attributed to excited-state absorption losses, with various possible processes. Such an effect has been previously studied for the role it plays in the lasing process of Ce^{3+}-containing tunable lasers (*28–30*).

Figure 21 compares the spectral distribu-

TABLE II

COMPARISON BETWEEN THE EMISSION CHARACTERISTICS OF SOME POWDERED CODOPED GLASSES AND THOSE OF THE STANDARD CALCIUM HALOPHOSPHATE PHOSPHOR $Ca_5(PO_4)_3(F,Cl)$: Sb^{3+},Mn^{2+}, UNDER A SIMILAR 254-nm EXCITATION

No.	Compositions	Chromaticity coordinates			Global intensity	Intensity corrected[a]
		x	*y*	*z*		
1	Li, Ba, 1% Ce_2O_3, 1% Tb_2O_3, 1% MnO	0.35	0.43	0.22	0.8	0.5
2	$67B_2O_3$, $15Li_2O$, 9BaO, $3Y_2O_3$, $2Al_2O_3$ $1As_2O_3$, $1Ce_2O_3$, $1Tb_2O_3$, 1MnO	0.36	0.44	0.20	0.8	0.5
3	Na, Ba, 1% Ce_2O_3, 1% Tb_2O_3, 1% MnO	0.32	0.41	0.27	0.6	0.4
4	Li, Ca, 1% Ce_2O_3, 1% Tb_2O_3, 1% MnO	0.36	0.44	0.20	0.9	0.5
5	$80B_2O_3$, $9.5Li_2O$, 5BaO, $1Al_2O_3$, $0.5As_2O_3$ $1La_2O_3$, $1Ce_2O_3$, $1Tb_2O_3$, 1MnO	0.40	0.49	0.11	1.1	0.6
6	$60B_2O_3$, $21.5Li_2O$, 10BaO, $2Al_2O_3$ $0.5As_2O_3$, $3La_2O_3$, $1Ce_2O_3$, $1Tb_2O_3$, 1MnO	0.32	0.39	0.29	0.7	0.4
S	$Ca_5(PO_4)_3(F,Cl)$: Sb,Mn	0.37	0.38	0.25	1	1

[a] Intensity was corrected by taking into account the standard observer's luminosity function.

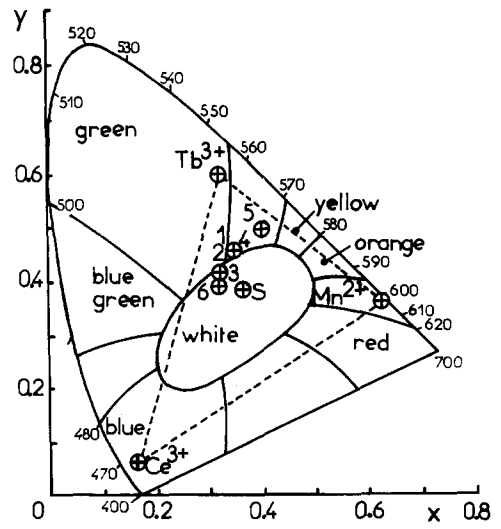

FIG. 22. Chromaticity coordinates characteristic of the emission of the samples listed in Table II, under 254-nm excitation.

tions of the emissions, under similar 254-nm excitation, of (Li, Ba, 1% Ce_2O_3, 1% Tb_2O_3, 1% MnO) ground glass and of the standard calcium halophosphate phosphor $Ca_5(PO_4)_3(F,Cl):Sb^{3+},Mn^{2+}$ (*1*). The integrated intensity of the glass emission is approximately 80% that of the phosphate. This value is reduced, however, down to 50% when taking into account the standard observer's luminosity function.

The chromaticity also varies by changing the glass composition or the activator concentrations. Some examples are listed in Table II and the corresponding representative points are reported on the chromaticity diagram (Fig. 22). All points mentioned are located within the triangle (dotted lines of Fig. 22) whose vertices represent the colors emitted by singly doped glasses. It is worthwhile to mention the unusual high saturation shown by the red emission of Mn^{2+} in these materials.

VIII. Concluding Remarks

Such materials, with better luminescence quantum yield, could be used in lighting devices or optical fibers.

The mechanism responsible for the strong dependence of Ce^{3+} emission intensity on excitation wavelength has to be identified as well as the contribution of exchange to the manganese excitation.

Several glass developments concerning also white light emitting materials combining the emission of only two activators or even doped with a single luminescent ion are at present in progress.

References

1. K. H. BUTLER, "Fluorescent Lamp Phosphors," Penn State Univ. Press, University Park (1980).
2. M. KOEDAM AND J. J. OPSTELTEN, *Lighting Res. Technol.* **3,** 205 (1971).
3. W. A. THORNTON, *J. Opt. Soc. Am.* **61,** 1155 (1971).
4. J. M. P. J. VERSTEGEN, D. RADIOLEVIC, AND L. E. VRENKEN, *J. Electrochem. Soc.* **121,** 1627 (1974).
5. B. SAUBAT, C. FOUASSIER, P. HAGENMULLER, AND J. C. BOURCET, *Mater. Res. Bull.* **16,** 193 (1981).
6. J. TH.W. DE HAIR AND J. T. C. VAN KEMENADE, Paper 54 presented at the 3rd International Symposium on Science and Technology of Light Sources, Toulouse, France, April 18–21 (1983).
7. B. LOOYE, J. TH. W. DE HAIR, AND C. BAKKER, European Patent NL 7905680 (23.07.79).
8. M. LESKELA, "Rare Earth Spectroscopy," pp. 617–628, World, Cleveland (1985).
9. J. TH. W. DE HAIR, *J. Lumin.* **18/19** (II), 797 (1979).
10. B. KELLENDONK AND G. BLASSE, *Phys. Status Solidi A* **73,** 205 (1982).
11. ZHANG JIN CHAO, C. PARENT, G. LE FLEM, AND P. HAGENMULLER, *C. R. Acad. Sci. Paris* **308** (II), 1335 (1989).
12. G. BLASSE AND A. BRIL, *Philips Tech. Rev.* **31**(10), 304 (1970).
13. P. F. BONGERS, *Philips Tech. Rev.* **28,** 13 (1967).
14. K. BINGHAM AND S. PARKE, *Phys. Chem. Glasses* **6**(6), 224 (1965).
15. Y. TANABE AND S. SUGANO, *J. Phys. Soc. Jpn.* **9,** 753 (1954).
16. P. E. MENASSA, D. J. SIMKIN, AND P. TAYLOR, *J. Lumin.* **35,** 223 (1986).
17. L. N. FEUERHELM, S. M. SIBLEY, AND W. A. SIBLEY, *J. Solid State Chem.* **54,** 164 (1984).
18. B. M. J. SMETS, *Mater. Chem. Phys.* **16**(3–4), 283 (1987).

19. D. L. DEXTER, *J. Chem. Phys.* **21**(5), 836 (1953).
20. P. BOCHU, C. PARENT, A. DAOUDI, G. LE FLEM, AND P. HAGENMULLER, *Mater. Res. Bull.* **16,** 883 (1981).
21. M. INOKUTI AND F. HIRAYAMA, *J. Chem. Phys.* **43,** 1978 (1965).
22. M. YOKOTA AND O. TANIMOTO, *J. Phys. Soc. Jpn.* **22**(3), 779 (1967).
23. TH. FÖRSTER, *Z. Naturforsch.* **4a,** 321 (1949).
24. M. V. ARTAMONOVA, CH. M. BRISKINA, A. I. BURSHTEIN, L. D. ZUSMAN, AND A. G. SKLEZNEV, *Sov. Phys. J.E.T.P.* **35**(3), 457 (1972).
25. YU. K. VORON'KO, T. G. MAMEDOV, V. V. OSIKO, A. M. PROKHOROV, V. P. SAKUN, AND I. A. SHCHERBAKOV, *Sov. Phys. J.E.T.P.* **44**(2), 251 (1976).
26. C. LURIN, C. PARENT, G. LE FLEM, AND P. HAGENMULLER, J., *Phys. Chem. Solids* **46**(9), 1083 (1985).
27. T. F. SOULES, R. L. BATEMAN, R. A. HEWES, AND E. R. KREIDLER, *Phys. Rev. B* **7,** 1657 (1973).
28. R. R. JACOBS, W. F. KRUPKE, AND M. J. WEBER, *Appl. Phys. Lett.* **33**(5), 410 (1978).
29. Y. ISHII, K. ARAI, H. NAMIKAWA, M. TANAKA, A. NEGISHI, AND T. HANDA, *J. Am. Ceram. Soc.* **70**(2), 72 (1987).
30. KI-SOO LIM AND D. S. HAMILTON, *J. Luminesc.* **40–41,** 319 (1988).